



Cite this: *New J. Chem.*, 2020, **44**, 16340

Development of phthalocyanine functionalised TiO₂ and ZnO nanofibers for photodegradation of methyl orange†

Sivuyisiwe Mapukata and Tebello Nyokong *

The photocatalytic activity of TiO₂ and ZnO based catalysts, which is based on their ability to generate electron–hole pairs upon photoillumination is limited due to their wide band gaps and lack of efficient retrievability post-application. This work reports on the fabrication, characterisation and comparison of electrospun TiO₂ and ZnO nanofibers when bare vs when functionalised with a phthalocyanine. The generated photocatalysts are attractive because they absorb visible light and are easily retrievable and hence reusable. With the Pc anchored onto their surfaces, the anatase TiO₂ nanofibers and the wurzite ZnO nanofibers possessed singlet oxygen quantum yields of 0.22 and 0.16 in water, respectively. Evaluation of the photocatalytic efficiencies of the nanofibers was conducted by studying the photodegradation of methyl orange. The Pc decorated nanofibers were found to be more effective photocatalysts than the bare ones with the phthalocyanine TiO₂ nanofibers being the best. The degradation kinetics were found to follow pseudo first order kinetics and obeyed the Langmuir Hinshelwood model. The nanocatalysts reported herein are therefore feasible candidates for real-life water purification applications.

Received 2nd July 2020,
 Accepted 11th September 2020

DOI: 10.1039/d0nj03326j

rsc.li/njc

Introduction

Over the years, research interest on semiconductor based photocatalysts has increased due to their versatile applications, including the photodegradation of organic waste, bacterial treatment, anti-cancer properties and water splitting.^{1–4} Titanium dioxide (TiO₂) and zinc oxide (ZnO) are the most commonly used of these photocatalysts due to their relatively low cost, good chemical and optical stability as well as their easy fabrication in a range of nanostructures such as nanowires, nanocombs and nanospheres *etc.*^{5–7} Both TiO₂ and ZnO however have wide band gaps of ~3.0 eV meaning their photoactivity is mainly under UV light.^{8,9} The sunlight reaching the earth's surface on the other hand only contains about 8% UV light, thereby limiting the real life applications of these photocatalysts.¹⁰

To combat that, this work reports on the fabrication of TiO₂ and ZnO nanofibers decorated with a zinc phthalocyanine (Pc). Pcs are versatile, intensely colored dyes containing four imino-isoinoline rings. They exhibit excellent visible/near infrared absorption, high chemical and thermal stability and the ability of generate singlet oxygen, which is the main active species in photocatalysis.^{11–13} Anchoring of Pcs on the TiO₂ and ZnO

nanofibers therefore yields fibers with two light absorbers, wherein the Pc absorbs visible light, which is beneficial as most of the solar irradiation is in the visible region.

The rationale behind choosing 2-[5-(phenoxy)-isophthalic acid]9(10),16(17),23(24)-tris(*tert*-butyl) phthalocyaninato zinc(II) (complex **1**, Fig. 1A) in this work is based on the fact that it has been reported that introducing diamagnetic metals such as Zn into the cavity of the Pc ring results in enhanced triplet and singlet oxygen quantum yields.^{14–16} It has also been reported that decreasing the symmetry of Pcs improves their singlet oxygen quantum yields.¹⁷

One of the essential requirements for the light-harvesting systems is that the sensitizer should possess directionality which can be achieved by using “push” (electron donating) and “pull” (electron withdrawing) functional groups as substituents on the Pc ring.¹⁸ Hence the chosen Pc also contains three *tert*-butyl and two carboxylic acid groups that act as “push” and “pull” groups, respectively. The carboxylic acid groups on the Pc also aid the anchoring of the Pc to the surface of TiO₂ or ZnO nanofibers to provide intimate electronic coupling between electrons in the lowest unoccupied molecular orbital (LUMO) of the Pc and the conduction band of the TiO₂ or ZnO.¹⁹ Lastly, the bulky *tert*-butyl groups will result in increased solubility and reduce aggregation of the Pc in solution.

The TiO₂ and ZnO nanofibers are fabricated through electrospinning and are attractive because they are easier to separate from solution than their liquid and powdered counterparts. Electrospinning is a fiber fabrication technique that exposes

Institute for Nanotechnology Innovation, Department of Chemistry, Rhodes University, Makhanda 6140, South Africa. E-mail: t.nyokong@ru.ac.za

† Electronic supplementary information (ESI) available. See DOI: 10.1039/d0nj03326j

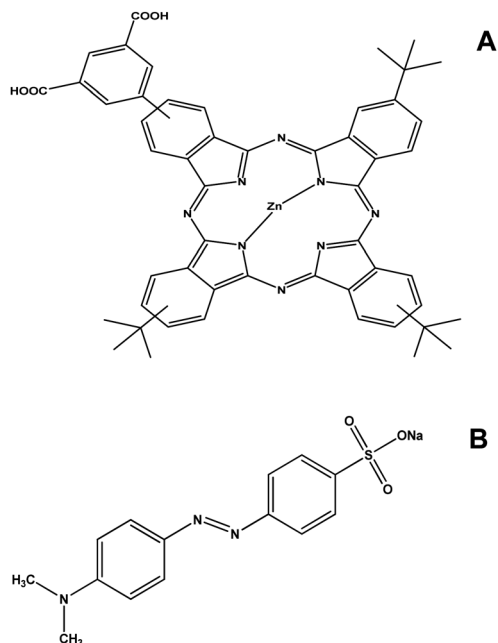


Fig. 1 Structure of (A) 2-[5-(phenoxo)-isophthalic acid]9(10),16(17),23(24)-tris(*tert*-butyl)phthalocyaninato zinc(II) (**1**) and (B) methyl orange (**MO**).

polymer droplets to high voltage resulting in the formation of fibers on a collector.²⁰ The formed fibers usually have small diameters (nano to micro scale) and high surface-to-volume ratios.^{21,22} Pcs have been employed in the presence of ZnO or TiO₂ materials for photocatalytic purposes when in suspension or embedded in electrospun fibers (the latter for ease of separation following use).^{23–25} The electrospun nanofibers reported in this work however are calcined with the aim of yielding regeneratable and possibly reusable catalysts. In addition, since no catalytic activity is associated with the polymer and it merely acts as a support, calcination of the fibers not only yields purely crystalline fibers but also eliminates the possible shielding of the activity of the embedded catalysts by the polymer.

In addition to the fabrication, characterisation and anchoring of a Pc on the surface of TiO₂ and ZnO nanofibers, their photocatalytic efficiencies on the degradation of organic pollutants are evaluated, using methyl orange (**MO**, Fig. 1B) as a model compound. **MO** is an azo dye that is widely used in industries including textiles, paper and leather amongst others.^{26,27} The release of dyes such as **MO** in the environment causes water pollution problems hence the importance of finding efficient means to eradicate them.

Experimental

Materials

Titanium propoxide, zinc acetate dihydrate, polyvinylpyrrolidone (PVP, $M_w = 1\,300\,000$) and anthracene 9,10-bis-methylmalonate (ADMA) were purchased from Sigma-Aldrich. All solvents were purchased from commercial suppliers and used as received.

The instrumentation used in the characterisation and analysis of the nanofibers can be found in the ESI.†

The synthesis of complex **1** (2-[5-(phenoxo)-isophthalic acid]-9(10),16(17),23(24)-tri-*tert*-butyl phthalocyaninato zinc(II), Fig. 1A) has been reported before.²⁸

Electrospinning method

Fabrication of TiO₂ nanofibers. Sample preparation and electrospinning were conducted as reported before.^{29,30} Briefly, a solution of 10% PVP in ethanol (10 mL) was prepared and to this solution, glacial acetic acid (5 mL) and titanium(IV) propoxide (10 mL) were added followed by stirring for 24 h. The resulting solution was then loaded into a syringe equipped with a stainless steel needle and connected to a high voltage power supply. An electric voltage of 12.5 kV was applied between the needle and the stationary aluminium foil collector with the distance between the tip of the needle and the collector being kept at 12 cm. The electrospinning was conducted at a flow rate was 1.5 mL h⁻¹ (controlled using a syringe pump) with the recorded temperature and humidity in the room being 25.7 °C and 52%, respectively. The collected composite nanofibers (PVP/TiO₂) were left in open air for 2 h and then calcined at 450 °C at a heating rate of 2 °C min⁻¹ for 3 h, thereby removing PVP which acts as a sacrificial polymer to obtain purely inorganic TiO₂ nanofibers.

Fabrication of ZnO nanofibers. The fabrication of the ZnO fibers was conducted as reported before but with slight modification.^{31,32} Briefly, zinc acetate (1.5 g) was dissolved in a solvent mixture of ethanol (15 mL) and dimethylformamide (DMF, 5 mL) under magnetic stirring at room temperature. After 2 h, PVP (2.5 g) was added to the solution followed by continuous stirring for 6 h to obtain a homogenous viscous solution. The solution was loaded into a plastic syringe equipped with a stainless steel needle and connected to a high voltage power supply. A solution flow rate of 0.03 mL h⁻¹ and a voltage of 15.5 kV were administered with the distance between the needle tip and the collector being maintained at 20 cm. The recorded temperature and humidity in the room were 26.7 °C and 49%, respectively. The electrospun composite nanofibers (PVP/ZnO) were collected on the surface of silicon substrates clamped on top of a conductive aluminium collector and subsequently exposed to the air overnight for stabilization. The PVP/ZnO nanofibers were calcined as explained above for the TiO₂ nanofibers to obtain purely inorganic ZnO nanofibers.

Anchoring of complex 1 on TiO₂ and ZnO nanofibers. Anchoring of the Pc on the surface of the nanofibers was conducted as reported before but with slight modification.³³ Complex **1** was dissolved in a 1 : 1 solvent mixture of acetonitrile and ethanol in two separate reaction vessels to make 75 μM solutions. The calcined TiO₂ and ZnO nanofibers were then each immersed in the individual Pc solutions overnight in sealed containers and left in the dark. Blue fibers were retrieved, washed with ethanol and then dried under a high vacuum fume hood. The resulting functionalised nanofibers are denoted **1-TiO₂** and **1-ZnO**, respectively.

Results and discussion

Characterisation

UV-vis spectroscopy. The UV-vis spectrum of complex **1** is shown in Fig. 2 wherein a prominent narrow Q band is observed,

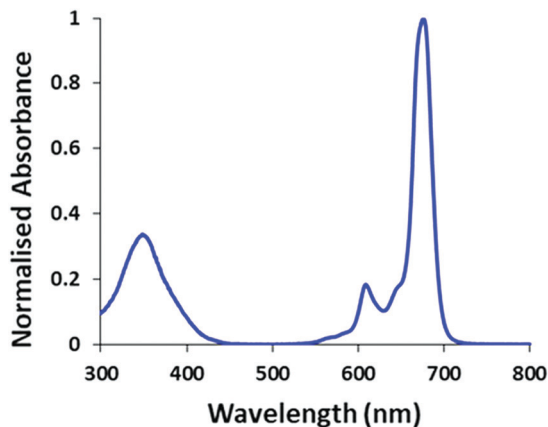


Fig. 2 Normalised UV-vis spectrum of complex **1** in DMSO.

attributed to the monomeric behaviour of the Pc in DMSO. The solid state UV-vis spectra of the bare and Pc functionalised nanofibers are shown in Fig. 3. The spectra of both the bare TiO_2 and ZnO nanofibers only exhibit absorption in the UV region, while the functionalised nanofibers (**1**- TiO_2 and **1**-ZnO nanofibers) exhibit additional absorption bands at 550–750 nm due to the presence of the Pc. The broadening of the Pc Q band is

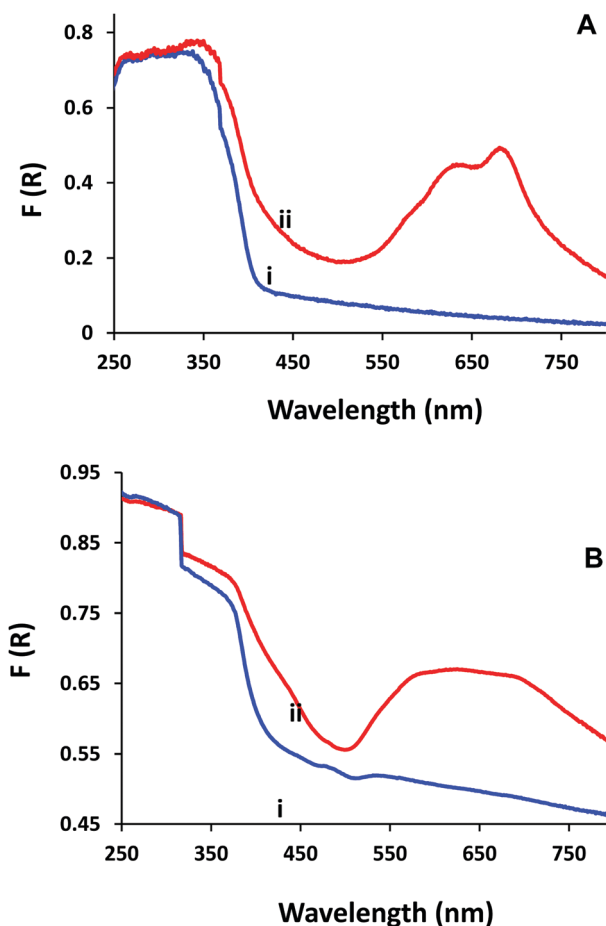


Fig. 3 Solid state UV-vis spectra of (A) (i) TiO_2 nanofibers (ii) **1**- TiO_2 nanofibers and (B) (i) ZnO nanofibers (ii) **1**-ZnO nanofibers.

due to aggregation and is typical for Pcs in the solid state.³⁴ The red shifting in the solid state compared to solution is also common for Pcs.³⁴

The band gap energy of complex **1** has been reported to be 1.83 eV³⁵ and those of the TiO_2 and ZnO nanofibers were calculated using the Tauc's eqn (1) as explained before.^{36,37}

$$(\alpha h\nu)^{1/n} = k(h\nu - E_g) \quad (1)$$

where α is the absorption coefficient, h is Planck's constant, ν is the photon's frequency, E_g is the band gap and k is a proportionality constant. The value of n in the exponent is an indication of the nature of the electronic transition and in the case of TiO_2 and ZnO, direct allowed transitions occur so $n = 1/2$.³⁶

The intercept of the linear fit of the Tauc plot (Fig. 4, using TiO_2 and **1**- TiO_2 nanofibers as examples) gives E_g . The Tauc plot shows that the estimated E_g for the TiO_2 nanofibers is approximately 3.19 eV (398 nm), similar to values reported before for anatase TiO_2 .³⁸ The E_g of **1**- TiO_2 is however lowered to 2.90 eV (415 nm), an indication of strong interaction between the Pc and TiO_2 . The estimated E_g for the ZnO nanofibers is 3.28 eV (389 nm), similar to values reported before for ZnO catalysts.³¹

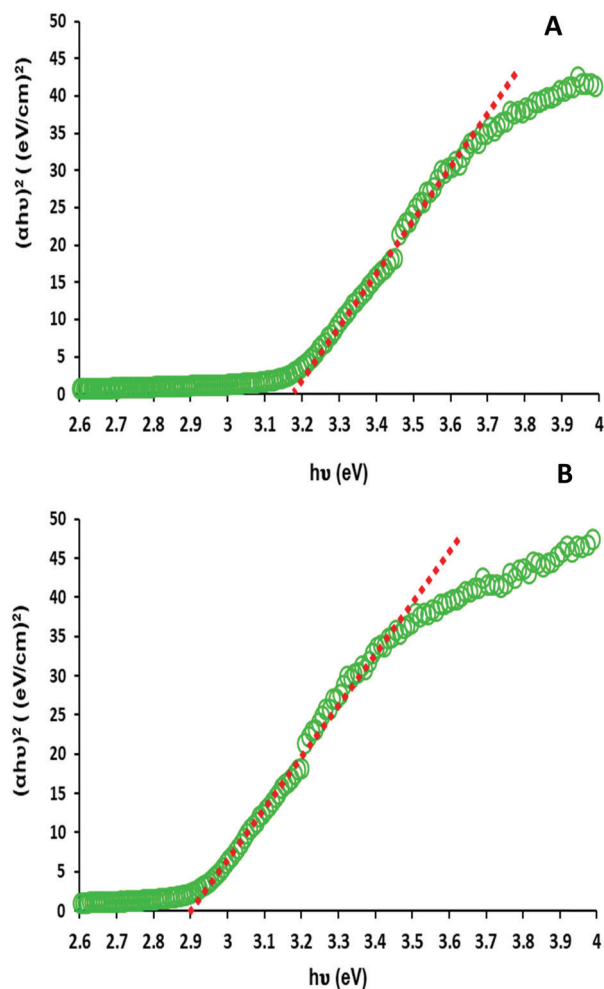


Fig. 4 Tauc plots for the determination of the E_g of (A) TiO_2 nanofibers and (B) **1**- TiO_2 nanofibers.

Just as with the TiO₂, the anchoring of the Pc to the nanofibers for 1-ZnO lowered the E_g to 3.00 eV (410 nm).

X-Ray diffraction spectroscopy. Phase identification of the different nanofibers was conducted using XRD. The XRD patterns of the nanofibers pre-calcination were also analysed as shown in Fig. 5A (using PVP/TiO₂ nanofibers pre-calcination as an example). The pattern shows that the uncalcined nanofibers are amorphous with a dominant broad peak at around $2\theta = 21^\circ$, which is attributed to the amorphous nature of PVP.³¹

Post-calcination, the diffraction patterns of both TiO₂ and ZnO nanofibers show pure crystallinity as demonstrated in Fig. 5B and C. The TiO₂ nanofibers show diffraction peaks at 25.39° , 37.93° , 48.26° , 54.13° , 55.28° , 62.88° , 69.21° , 70.50° and 75.30° corresponding to the (101), (004), (200), (105), (211), (204), (116), (220) and (215) tetragonal planes of anatase TiO₂ (JCPDS card no. 78-2486). Confirmation of the anatase phase of the TiO₂ nanofibers is advantageous because unlike the other crystallographic structures of TiO₂ *i.e.* rutile (tetragonal), and brookite (orthorhombic), the tetragonal anatase is metastable at ambient temperature and possesses the highest photocatalytic

activity compared to the others.³⁹ This can be attributed to its adsorption affinity for organic molecules and a lower electron-hole recombination rate.⁴⁰ The ZnO nanofibers show diffraction peaks at 2θ values of 31.72° , 34.46° , 36.94° , 47.86° , 56.78° , 63.76° , 68.96° and 69.70° , corresponding to the (100), (002), (101), (102), (110), (103), (112) and (201) planes of hexagonal wurzite of crystalline ZnO (JCPDS card no. 36-1451).⁴¹ This means that there is a close packing of oxygen and zinc atoms in tetrahedral sites, which gives rise to the typical crystal habit of ZnO.³¹

Fourier-transform infrared (FT-IR) spectroscopy

FT-IR spectroscopy was used to confirm complete removal of the PVP from the nanofibers as well as efficient anchoring of the Pc on their surface. As shown in Fig. 6A, the spectrum of the nanofibers pre-calcination (using PVP/TiO₂ nanofibers as an example) shows a series of peaks including those at 1248 cm^{-1} (C–N stretch), 1419 cm^{-1} (C–H bend), 1656 cm^{-1} (C=O stretch) and 2945 cm^{-1} (C–H stretch) due to the presence PVP. There is also a broad peak at 3485 cm^{-1} , attributed to the surface adsorbed water and hydroxyl groups on the PVP.⁴²

Post-calcination, none of the polymer peaks are maintained, instead the TiO₂ nanofibers show peaks at 475 cm^{-1} and 730 cm^{-1} (Fig. 6B) attributed to the O–Ti–O bonding in anatase morphology.^{39,43} There is also a peak at 3390 cm^{-1} due to the adsorbed hydroxyl groups on the TiO₂ surface. This proves that the TiO₂ nanofibers are purely inorganic. Similar results were observed for the ZnO nanofibers (Fig. 6C) as a single peak at 368 cm^{-1} was observed corresponding to the vibration of hexagonal ZnO.⁴⁴ Successful anchoring of the Pc on the surface of the nanofibers was also proven as demonstrated in Fig. 6D (using 1-TiO₂ nanofibers as an example). The spectrum shows peaks at 1332 cm^{-1} (C–N stretch), 1730 cm^{-1} (C=O stretch) and 3280 cm^{-1} (O–H stretch) attributed to the presence of the Pc and the characteristic O–Ti–O peaks at 485 and 738 cm^{-1} , showing that the Pc is efficiently anchored on the surface of the nanofibers. A similar spectrum was observed for the 1-ZnO nanofibers (not shown).

Scanning electron microscopy

Analysis of the surface topography of the nanofibers was conducted using SEM. As shown in Fig. 7A, the PVP/TiO₂ nanofibers are branched and cylindrical with smooth surfaces. Post calcination however, the nanofibers are coiled with broken edges and there is a shrinkage in size due to the removal of the PVP (Fig. 7B). The PVP/ZnO nanofibers on the other hand are unbranched, cylindrical and have smooth surfaces (Fig. 7C). Post calcination, there is an observed shrinkage of the nanofibers, also attributed to the removal of PVP. The nanofibers are also branched and interconnected with more rough and uneven surfaces.

Brunauer–Emmett–Teller (BET)

BET was performed so as to determine the pore sizes and surface areas of the nanofibers before and after anchoring of the Pc. A high surface area is an important attribute in the design of photocatalysts because a large surface area will provide more active sites thereby enhancing the absorption of

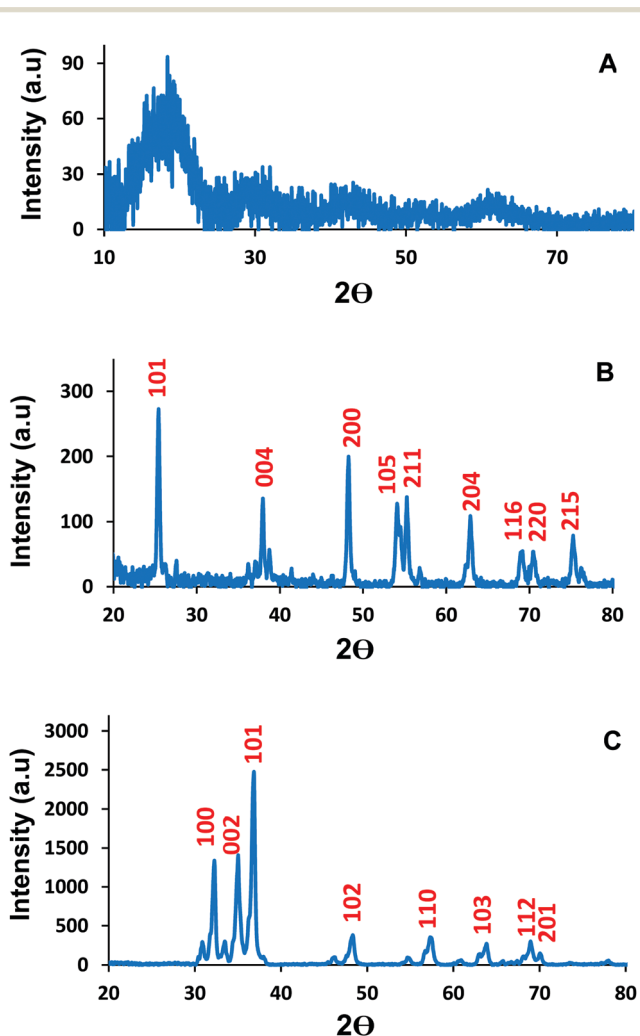


Fig. 5 XRD patterns of (A) PVP/TiO₂ nanofibers, (B) TiO₂ nanofibers and (C) ZnO nanofibers.

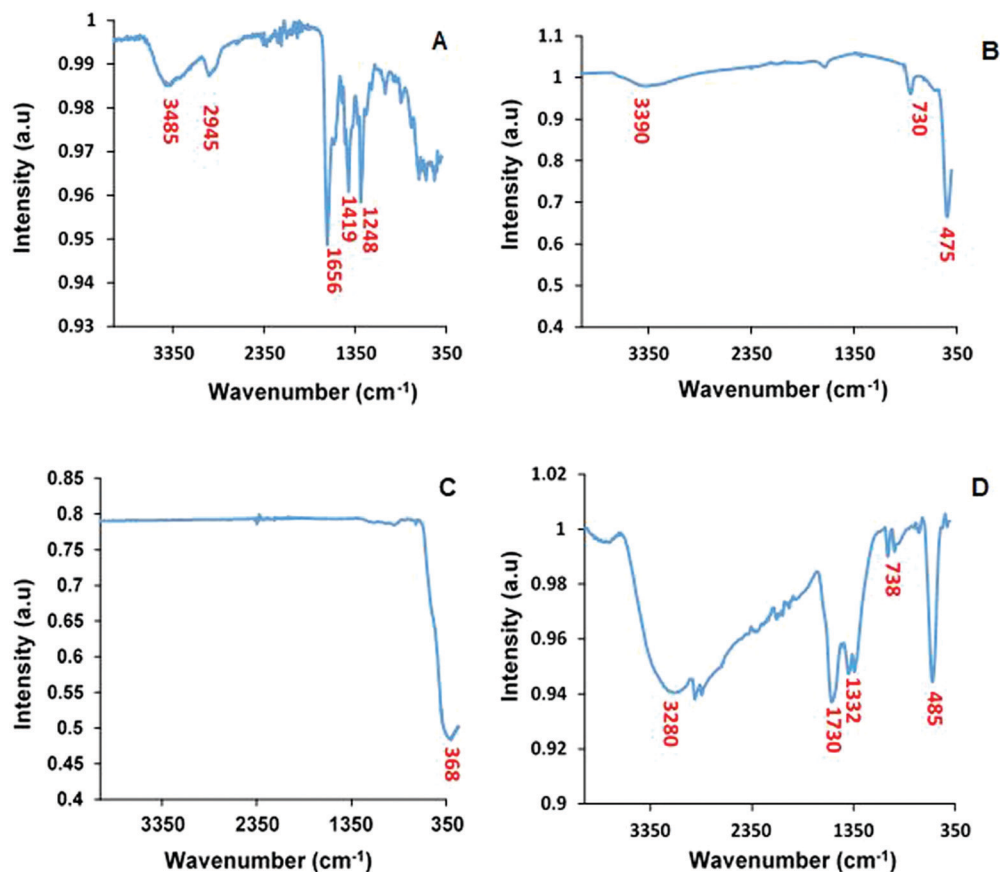


Fig. 6 FT-IR spectra of (A) PVP/TiO₂ nanofibers, (B) TiO₂ nanofibers, (C) ZnO nanofibers and (D) 1-TiO₂ nanofibers.

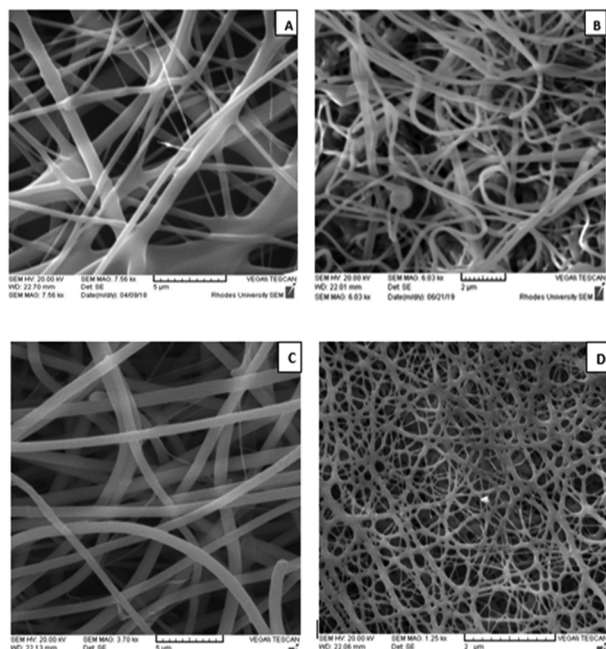


Fig. 7 (A) SEM images of (A) PVP/TiO₂ nanofibers, (B) TiO₂ nanofibers, (C) PVP/ZnO nanofibers and (D) ZnO nanofibers.

photons and adsorption of the MO on the surface of the catalyst.⁴⁵ The pore volume and surface areas of the nanofibers

are listed in Table 1. The results show that anchoring of the Pc on the surface of the bare TiO₂ and ZnO nanofibers results in a decrease in the surface area and pore volume. Rough surfaces have been reported to possess larger surface areas than smooth ones.⁴⁶ This can therefore suggest that the roughness of the nanofibers is reduced in the presence of the Pc (1-TiO₂ and 1-ZnO nanofibers).

The observed decrease in the pore volume can be attributed to the Pc molecules being entrapped and filling the pores of the nanofibers. In addition, a higher surface area and pore volume is observed for the 1-TiO₂ nanofibers relative to the 1-ZnO nanofibers. The BET isotherms of the 1-TiO₂ and 1-ZnO are shown in Fig. 8. The results show that the nanofibers exhibit type IV BET isotherm with a hysteresis loop, proving the existence of mesopores on the nanofibers. The type IV isotherm also indicates an indefinite multilayer formation after completion of the monolayer.⁴⁷

Singlet oxygen quantum yield

As mentioned before, singlet oxygen is one of the main active species in photocatalysis. It is therefore of importance to determine the singlet oxygen generating efficiency of the Pc decorated nanofibers (1-TiO₂ and 1-ZnO nanofibers). Singlet oxygen quantum yield (Φ_{Δ}) calculations were carried out in unbuffered aqueous media wherein ADMA was used as a quencher with its degradation being monitored at 380 nm. The equations that were used for the

Table 1 BET properties and Langmuir–Hinshelwood kinetic data of the electrospun bare and modified ZnO and TiO₂ fibers

Catalyst	Surface area (m ² g ⁻¹)	Pore volume (cm ³ g ⁻¹)	Φ_{Δ}	Langmuir–Hinshelwood parameters ^a		
				k (10 ⁻⁷) (mol L ⁻¹ min ⁻¹)	K_A (10 ⁴) (mol ⁻¹ L)	R^2
Complex 1	—	—	0.57 ²⁸ (DMSO)	—	—	—
TiO ₂ nanofibers	13.40	0.190	—	2.57 (2.34)	3.86 (3.85)	0.967 (0.941)
1-TiO ₂ nanofibers	12.70	0.110	0.22 (water)	4.22 (3.72)	4.49 (4.83)	0.984 (0.993)
ZnO nanofibers	11.36	0.240	—	2.18 (2.06)	4.08 (4.05)	0.986 (0.980)
1-ZnO nanofibers	10.45	0.080	0.16 (water)	3.71 (3.59)	4.30 (4.18)	0.994 (0.994)

^a Values in brackets are for the results obtained for the reused catalysts.

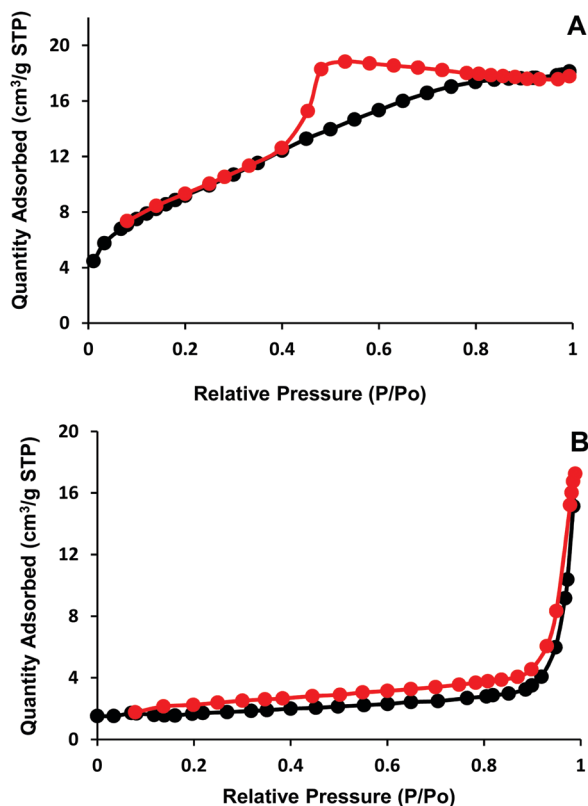


Fig. 8 BET isotherms of (A) 1-TiO₂ nanofibers and (B) 1-ZnO nanofibers. Black curve = adsorption and red curve = desorption.

calculations of the Φ_{Δ} are included in the ESI.† The Φ_{Δ} of complex 1 in dimethyl sulfoxide (DMSO) is 0.57.²⁸ The spectrum showing the degradation of ADMA in the presence of the functionalised nanofibers is shown in Fig. 9 (using 1-TiO₂ nanofibers as an example). Low Φ_{Δ} of 0.22 and 0.16 were calculated for the 1-TiO₂ and 1-ZnO nanofibers, respectively.

This is not surprising as oxygen has a higher solubility in many organic solvents compared to water.⁴⁸ Based on the ability of the 1-TiO₂ and 1-ZnO nanofibers to generate singlet oxygen which is necessary for photooxidation of organic pollutants, their photocatalytic abilities were compared to their bare counterparts (TiO₂ and ZnO nanofibers) in the degradation of MO.

Photostability studies

With the long-term photostability of TiO₂ and ZnO having been reported before,^{31,39} in this work the photostability of complex

1 was determined using photodegradation studies (Φ_{Pd}) where the Pc was degraded under light irradiation.⁴⁹ This is especially important for Pc complexes intended for use as photocatalysts.⁵⁰ The equation that was used for the calculation of the photodegradation quantum yield of complex 1 is included in the ESI.† For unstable complexes, the Φ_{Pd} values are of the order of 10⁻³.⁵¹ Complex 1 is relatively stable in DMSO as its Φ_{Pd} was calculated to be 10.3 × 10⁻⁶. The photodegradation spectrum also reveals that there was only a slight decrease observed in the intensities of both the Q and B bands with irradiation (Fig. S1, ESI†). There are also no changes in the shape of the spectrum with irradiation, thereby confirming that no phototransformation of the Pc into another absorbing species occurs during the irradiation process.

Photodegradation of MO

Spectral changes. The photocatalytic efficiencies of the bare and Pc decorated nanofibers were evaluated and compared with the aim of creating heterogeneous catalysts for easy recovery and hence reusability. A halogen lamp was used as the light source as it produces a continuous spectrum of light, from the near ultraviolet and visible regions to infrared irradiation (320–1100 nm), much like solar irradiation. The photodegradation studies were conducted in aqueous solutions at pH 2.5 because it has been reported that the degradation of MO is enhanced in acidic conditions with pH ranges of 2–3.^{52,53} The spectral changes that occurred during the exposure of MO to the nanofibers are shown and Fig. 10 (using 1-TiO₂ nanofibers as an example).

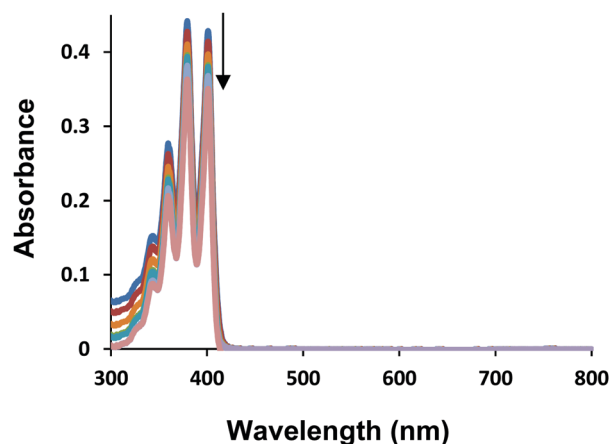


Fig. 9 UV/vis spectra changes of ADMA in water in the presence of 1-TiO₂ nanofibers.

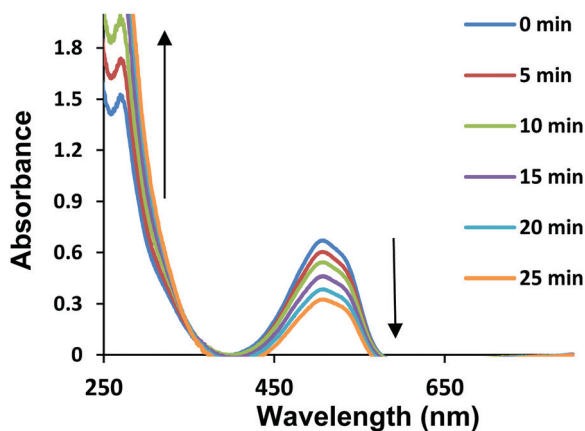


Fig. 10 UV/vis spectral changes in the photodegradation of 1.44×10^{-5} M **MO** using **1-TiO₂** nanofibers at pH 2.5 with 5 min irradiation intervals.

The spectrum proves that indeed the pollutant does not just adsorb on the surface of the fibers but is degraded and transformed into something else. There is an observed decrease in the intensity of the absorption peaks at 506 nm which is attributed to the azo bond. This explains the observed fading in the colour of the **MO** solution with increased irradiation time. The azo bond determines the colour of the dyes and is very reactive usually undergoing oxidation hence leading to fading of their colour.⁵⁴ The spectrum also shows an increase in the peaks below 330 nm which have been attributed to the presence of benzene rings.⁵⁵ This therefore suggests that the benzene rings remain intact and are not degraded during the photodegradation of **MO**. Similar spectral changes were observed when the other nanofibers were applied (not shown). No spectral changes were observed when studies were conducted in the absence of irradiation and oxygen (*i.e.* nitrogen purged solutions). This is an indication that light and molecular oxygen are prerequisites for the photodegradation process.

Kinetics studies

The photocatalytic degradation of **MO** was conducted on five different concentrations: 1.44×10^{-5} , 2.80×10^{-5} , 3.70×10^{-5} , 4.45×10^{-5} and 6.6×10^{-5} mol L⁻¹. The kinetic plots for the degradation of **MO** are shown in Fig. 11A (using studies conducted with **1-TiO₂** nanofibers as examples, and some of the concentrations). The plots are well fitted by a mono-exponential curve, suggesting that degradation using the nanofibers follows pseudo first order kinetics as observed before in the degradation of **MO** with TiO₂ and ZnO based catalysts.^{56,57} The kinetic data for the degradation of **MO** using the bare nanofibers (TiO₂ and ZnO) and the Pc decorated nanofibers (**1-TiO₂** and **1-ZnO**) is listed in Tables 2 and 3, respectively.

The obtained kinetics data shows that the rate constant (k_{obs}) decreases with increase in the concentration while the half-lives ($t_{1/2}$) increased. This basically means that for the same irradiation time, the relative amount of **MO** decomposed is less for the more concentrated solutions.⁵⁸ Comparison of the degradation efficiencies of the bare relative to the Pc decorated nanofibers as shown in Tables 2 and 3 depicts that the

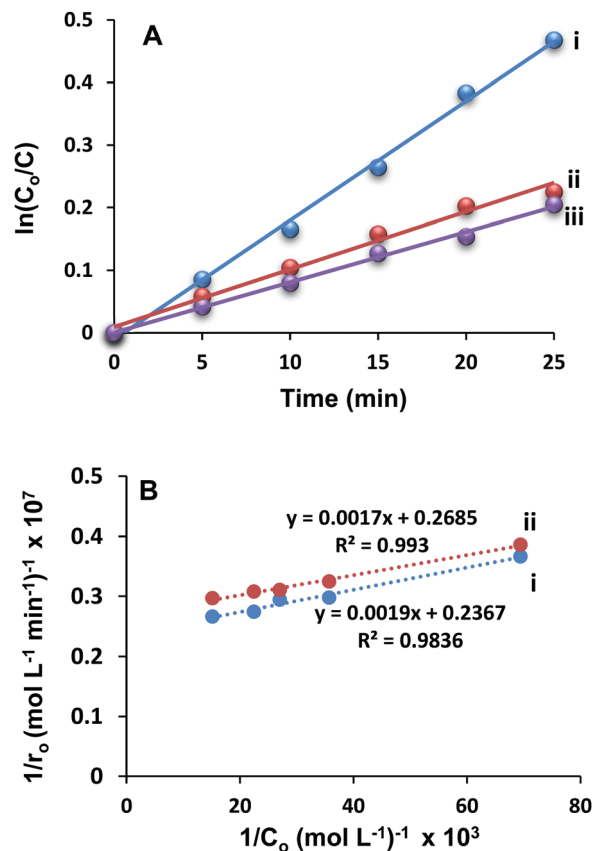


Fig. 11 (A) Pseudo first order kinetics plot for the degradation of (i) 1.44×10^{-5} , (ii) 3.70×10^{-5} and (iii) 4.45×10^{-5} mol L⁻¹ **MO** using **1-TiO₂** nanofibers at pH 2.5. (B) Plots of the reciprocal of the initial rate of degradation against the reciprocal of the concentration of **MO** using (i) the fresh **1-TiO₂** nanofibers and (ii) reused **1-TiO₂** nanofibers.

decorated nanofibers are better photocatalysts than the bare ones. This can be attributed to the bare TiO₂ and ZnO nanofibers having band gap energies of 3.19 and 3.28 eV, respectively showing their limited range of light absorption. The **1-TiO₂** and **1-ZnO** nanofibers on the other hand have two light absorbers and have band gap energies that extend into the visible region. In addition, the poorer activity of the ZnO nanofibers relative to TiO₂ nanofibers can be attributed to the dissolution and photo-dissolution of ZnO under acidic conditions.⁵⁹ Comparison of the Pc decorated nanofibers shows that the **1-TiO₂** nanofibers possess better photoactivity than the **1-ZnO** nanofibers, results which correlate to their respective singlet oxygen generation efficiencies. Furthermore, the **1-TiO₂** nanofibers have a higher surface area than the **1-ZnO** and it has been reported that increased catalyst surface area can enhance its photocatalytic activity.⁴⁵ Due to the easy retrievability of the nanofibers post application, the nanofibers were rinsed with water followed by ethanol and then dried in a high vacuum fumehood overnight. The nanofibers were then reapplied and as seen in Tables 2 and 3, there was a slight reduction in the photodegradation efficiency of all the nanofibers upon reuse. The loss in photoactivity can possibly be due to the adsorption of degraded species on the photocatalyst surface resulting in the blocking of some active sites.⁶⁰

Table 2 Kinetic data for the degradation of MO using TiO₂ and ZnO nanofibers at pH 2.5

[MO] × 10 ⁻⁵ (mol L ⁻¹)	<i>k</i> _{obs} (min ⁻¹)		Rate (10 ⁻⁷ mol L ⁻¹ min ⁻¹)		<i>t</i> _{1/2} (min)	
	TiO ₂	ZnO	TiO ₂	ZnO	TiO ₂	ZnO
1.44	0.0099 (0.0090)	0.0089 (0.0083)	1.43 (1.30)	1.28 (1.20)	70.00 (77.00)	77.87 (83.49)
2.80	0.0069 (0.0063)	0.0056 (0.0052)	1.93 (1.76)	1.57 (1.46)	100.4 (110.0)	123.8 (133.3)
3.70	0.0054 (0.0051)	0.0047 (0.0045)	2.00 (1.89)	1.74 (1.67)	128.3 (135.9)	147.4 (154.0)
4.45	0.0046 (0.0041)	0.0041 (0.0037)	2.05 (1.82)	1.82 (1.65)	157.5 (169.0)	169.0 (187.3)
6.60	0.0032 (0.0029)	0.0028 (0.0027)	2.11 (1.91)	1.85 (1.78)	216.6 (239.0)	247.5 (256.7)

Values in brackets are for the results obtained for the reused catalysts.

Table 3 Kinetic data for the degradation of MO using 1-TiO₂ and 1-ZnO nanofibers at pH 2.5

[MO] × 10 ⁻⁵ (mol L ⁻¹)	<i>k</i> _{obs} (min ⁻¹)		Rate (10 ⁻⁷ mol L ⁻¹ min ⁻¹)		<i>t</i> _{1/2} (min)	
	1-TiO ₂	1-ZnO	1-TiO ₂	1-ZnO	1-TiO ₂	1-ZnO
1.44	0.019 (0.018)	0.016 (0.015)	2.73 (2.59)	2.30 (2.16)	36.47 (38.50)	43.31 (46.2)
2.80	0.012 (0.011)	0.0099 (0.0094)	3.36 (3.08)	2.77 (2.63)	57.75 (63.00)	70.00 (73.72)
3.70	0.0092 (0.0087)	0.0080 (0.0076)	3.40 (3.22)	2.96 (2.81)	75.32 (79.66)	86.63 (91.18)
4.45	0.0080 (0.0073)	0.0070 (0.0067)	3.65 (3.25)	3.12 (2.98)	86.63 (94.93)	99.00 (103.4)
6.60	0.0057 (0.0051)	0.0050 (0.0048)	3.76 (3.37)	3.30 (3.17)	121.6 (135.9)	138.6 (144.4)

Values in brackets are for the results obtained for the reused catalysts.

The relationship between the concentration and rate of degradation of organic pollutants in heterogeneous photocatalytic reactions such as those reported herein can be expressed using the Langmuir–Hinshelwood model. The model has been successfully employed to describe kinetics of solid–liquid reactions in the degradation of various pollutants using TiO₂ and ZnO based catalysts.^{56,61} This model basically suggests that during the photocatalytic process, the reactants adsorb onto the surface of the catalyst in the first step followed by reactions between the adsorbed reactants.⁶² This entails the oxidation of the dye through attacks by the various reactive oxygen species (ROS) (including singlet oxygen) from the photocatalysts.

The Langmuir–Hinshelwood kinetic model is demonstrated in eqn (2):

$$\frac{1}{r_0} = \frac{1}{kK_A} \frac{1}{C_0} + \frac{1}{k} \quad (2)$$

where *r*₀ is the initial photocatalytic degradation rate (mol L⁻¹ min⁻¹), *C*₀ is the initial concentration of MO (mol L⁻¹), *k* is the apparent reaction rate constant (mol L⁻¹ min⁻¹) and *K*_A is the adsorption coefficient (mol⁻¹ L).⁶⁰

Plots of the reciprocal of the initial rate of degradation against the reciprocal of the concentration of MO for all the photocatalysts were found to be linear with non-zero intercepts (Fig. 11B, using studies conducted with 1-TiO₂ nanofibers as examples). This is confirmation that the degradation of MO using the bare and Pc decorated nanofibers under the reported conditions obeys the Langmuir–Hinshelwood kinetics model. The apparent rate constants (*k*) and adsorption coefficient (*K*_A) were obtained from the *y*-intercepts and slopes of the lines, respectively. As shown in Table 1, higher *K*_A values are obtained for 1-TiO₂ and 1-ZnO nanofibers than the bare TiO₂ and ZnO nanofibers, possibly due to the π–π interaction between the Pc and MO which enhances its adsorption onto the surface to the nanofibers. The results also show that the 1-TiO₂ nanofibers

have higher *K*_A values than the 1-ZnO nanofibers. This is an indication that the adsorption of MO mostly favours the 1-TiO₂ nanofibers, their larger surface area as explained with BET being a possible reason for this. The results also show that *K*_A is slightly higher for the reused 1-TiO₂ nanofibers rather than the fresh one while the opposite is observed for the 1-ZnO nanofibers.

This therefore demonstrates that for the reaction conditions implemented herein, the reusability of the 1-TiO₂ nanofibers is more favoured than that of the 1-ZnO nanofibers. The observation of photocatalysis on the re-used nanofibers confirms their integrity is maintained. In addition, the UV-vis spectra of the nanofibers before and after use (Fig. S2, ESI† using 1-TiO₂ nanofibers as an example) shows very little change in the Q band intensity confirming the stability of the Pc following use.

Mechanism

When the bare TiO₂ and ZnO nanofibers are exposed to UV light (from halogen lamp), electrons are transferred from the valence band to the conduction band, thereby leaving behind holes in the valence band and thus forming electron–hole pairs. The generated electrons and holes can reduce and oxidize the reactants which are adsorbed by the semiconductors, respectively.⁶³ The photo-generated holes facilitate the formation of hydroxyl radicals by the oxidation of OH⁻ and H₂O molecules which are adsorbed on the surfaces of the semiconductor. These photo-produced hydroxyl radicals in turn oxidize and degrade organic materials such as MO.⁶⁴

Decoration of the nanofibers with a Pc however yields a system wherein the TiO₂/ZnO primarily acts as an electron transfer agent and the Pc acts as a photosensitizer.³⁷ The mechanism of degradation of MO using a halogen lamp with semiconductor-Pc based photocatalysts is depicted in Fig. 12 (using 1-TiO₂ as an example). The process is initiated by the excitation of the Pc thereby generating electrons and photo-generated holes in the lowest unoccupied molecular orbital

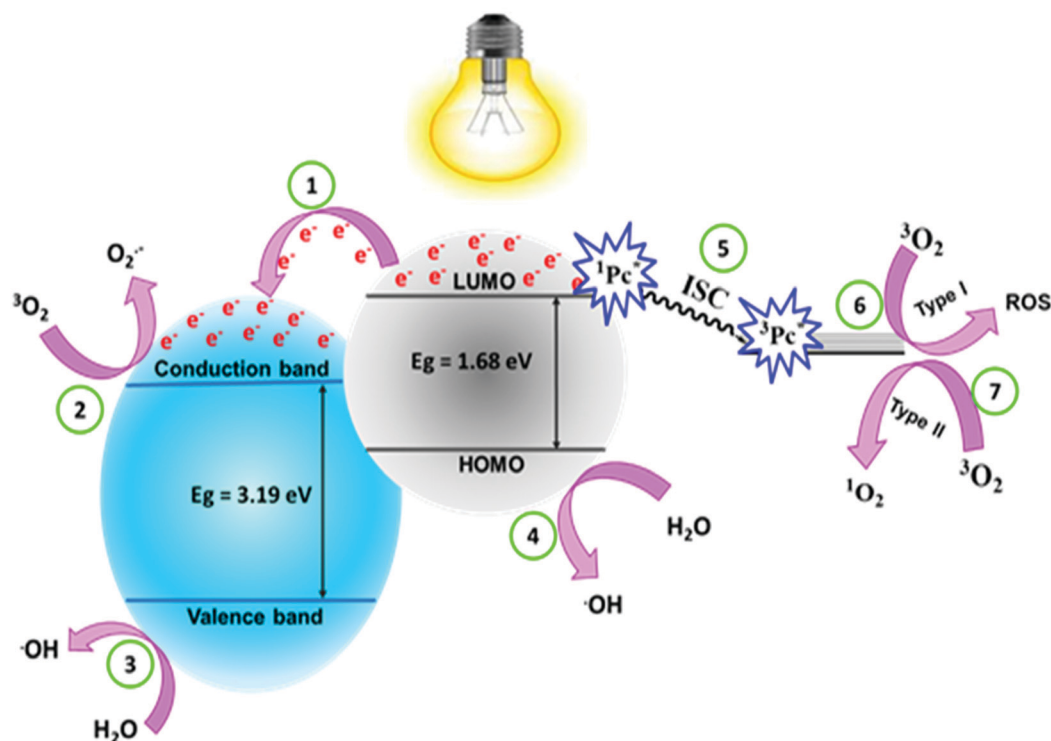


Fig. 12 Mechanism of degradation of methyl orange using 1-TiO₂ nanofibers. ISC = intersystem crossing, LUMO = lowest unoccupied molecular orbital, HOMO = highest occupied molecular orbital and ROS = reactive oxygen species.

(LUMO) and highest occupied molecular orbital (HOMO) of the Pc, respectively. The electrons in the LUMO are then injected into the conduction band of TiO₂ (path 1). The electrons in the conduction band of TiO₂ react with molecular oxygen to generate reactive superoxide anion radical (path 2). The holes in the valence band of TiO₂ react with the adsorbed water molecules on the surface of the photocatalyst to generate hydroxyl radicals (path 3). Simultaneously, the radical cation of the Pc that is formed during its excitation, reacts with water that is present at the surface of the photocatalyst to generate strongly oxidizing hydroxyl radicals (path 4).^{37,65} In another process, the photosensitizer in its singlet excited state undergoes intersystem crossing to the forbidden triplet excited state (path 5). Subsequent reactions result in the formation of ROS (path 6) and singlet oxygen (path 7) through electron and energy transfer, respectively.⁶⁶ The generated ROS, singlet oxygen and hydroxyl radicals from the interaction of the catalysts are strong oxidizing agents that can decompose organic pollutants.⁶⁷

Conclusions

The fabrication and characterisation of bare and Pc decorated TiO₂ and ZnO nanofibers has been successfully conducted, with the aim of creating heterogenous photocatalysts for degrading common organic water pollutants. These nanofibers are especially attractive due to their ability to absorb UV and visible light as well as their retrievability and hence reusability post-application. Low singlet oxygen quantum yields of 0.22 and 0.16 were quantified for 1-TiO₂ and 1-ZnO, respectively.

The photocatalytic efficiencies of the nanofibers were evaluated based on their ability to degrade MO wherein the Pc decorated nanofibers were found to be more effective with the 1-TiO₂ nanofibers being the best. The photocatalysis kinetics showed that the degradation of MO using the TiO₂ and ZnO nanofibers follows pseudo first order kinetics and obeys the Langmuir-Hinshelwood model. The nanofibers reported herein are therefore good candidates for applications as real-life water purification catalysts, even more so when modified with a zinc Pc.

Conflicts of interest

There are no conflicts to declare.

Acknowledgements

This work was supported by the department of Science and Technology, Republic of South Africa and National Research Foundation through DST/NRF South Africa Research Chairs Initiative for Professor of Medicinal Chemistry and Nanotechnology (Grant number UID 62620) and Rhodes University.

References

- 1 A. O. Ibhaddon and P. Fitzpatrick, *Catalysts*, 2013, 3, 189–218.
- 2 S. Gosh, V. S. Goudar, K. G. Padmalekha, S. V. Bhat, S. S. Indi and H. N. Vasan, *RSC Adv.*, 2012, 2, 930–940.

- 3 H. Yin, P. S. Casey, M. J. McCall and M. Fenech, *Langmuir*, 2010, **19**, 15399–15408.
- 4 J. Tang, J. R. Durrant and D. R. Klug, *J. Am. Chem. Soc.*, 2008, **130**, 13885–13891.
- 5 D. J. Mowbray, J. I. Martinez, J. M. García Lastra, K. S. Thygesen and K. W. Jacobsen, *J. Phys. Chem. C*, 2009, **113**, 12301–12308.
- 6 M. Willander, Q. X. Zhao, Q.-H. Hu, P. Klason, V. Kuzmin, S. M. Al-Hillib, O. Nur and Y. E. Lozovik, *Superlattices Microstruct.*, 2008, **43**, 352–361.
- 7 S. Hernández, D. Hidalgo, A. Sacco, A. Chiodoni, A. Lamberti, V. Cauda, E. Tresso and G. Saracco, *Phys. Chem. Chem. Phys.*, 2015, **17**, 7775–7786.
- 8 X. Yu, T. Hou, Y. Li, X. Sun and S.-T. Lee, *Int. J. Quantum Chem.*, 2013, **113**, 2546–2553.
- 9 U. S. Nur, F. C. Thye, Y. K. Kuan, R. Y. Mohd and K. N. G. Inn, *Mater. Sci. Forum*, 2016, **888**, 309–313.
- 10 F. J. Barbero, G. Lopez and F. J. Batlles, *Ann. Geophys.*, 2006, **24**, 2105–2114.
- 11 D. Mondal and S. Bera, *Adv. Nat. Sci.: Nanosci. Nanotechnol.*, 2014, **5**, 1–14.
- 12 *The Porphyrin Handbook*, ed. K. M. Kadish, K. M. Smith and R. Guillard, Academic Press, San Diego, 2003.
- 13 D. Mondal and S. Bera, *Adv. Nat. Sci.: Nanosci. Nanotechnol.*, 2014, **5**, 1–14.
- 14 M. Durmus and T. Nyokong, *Tetrahedron*, 2007, **63**, 1385–1394.
- 15 R. Bonnett, *Chemical Aspects of Photodynamic Therapy*, Gordon and Breach Science Publishers, Amsterdam, 2000.
- 16 N. Masilela and T. Nyokong, *J. Lumin.*, 2010, **130**, 1787–1793.
- 17 *Photodynamic tumor therapy: 2nd and 3rd generation photosensitizers*, ed. A. Weitemeyer, H. Kleish, U. Michelsen, A. Hirtb, D. Wöhrle and G. Moser, Harwood Academic Publishers, The Netherlands, 1998, ch. 2.
- 18 L. Giribabu, C. V. Kumar, V. G. Reddy, P. Y. Reddy, C. S. Rao, S.-R. Jang, J.-H. Hum, M. K. Nazeeruddin and M. Grätzel, *Sol. Energy Mater. Sol. Cells*, 2007, **91**, 1611–1616.
- 19 L. Zhang and J. M. Cole, *ACS Appl. Mater. Interfaces*, 2015, **7**, 3427–3455.
- 20 N. Bhardwaj and S. C. Kundu, *Biotechnol. Adv.*, 2010, **28**, 325–347.
- 21 S. V. Fridrikh, J. H. Yu, M. P. Brenner and G. C. Rudledge, *Phys. Rev. Lett.*, 2003, **90**, 1–4.
- 22 D. H. Reneker and I. Chun, *Nanotechnology*, 1996, **7**, 216–223.
- 23 X. Wang, J. Gao, B. Xu, T. Hua and H. Xia, *RSC Adv.*, 2015, **5**, 87233–87240.
- 24 H. You and Y. Zhao, *J. Phys. Chem. Biophys.*, 2016, **6**, 1000199.
- 25 P. Khoza and T. Nyokong, *J. Coord. Chem.*, 2015, **68**, 1117–1131.
- 26 M. B. Alqaragully, *Int. J. Adv. Res. Chem. Sci.*, 2014, **1**, 48–59.
- 27 J. Ma, F. Yu, L. Zhou, L. Jin, M. Yang, J. Luan, Y. Tang, H. Fan, Z. Yuan and J. Chen, *ACS Appl. Mater. Interfaces*, 2012, **4**, 5749–5760.
- 28 S. Mapukata, N. Kobayashi, M. Kimura and T. Nyokong, *J. Photochem. Photobiol., C*, 2019, **379**, 112–122.
- 29 B. Caratão, E. Carneiro, P. Sá, B. Almeida and S. Carvalho, *J. Nanotechnol.*, 2014, 1–5.
- 30 D. Li and Y. Xia, *Nano Lett.*, 2003, **3**, 555–560.
- 31 A. Di Mauro, M. Zimbone, M. E. Fragalà and G. Impellizzeri, *Mater. Sci. Semicond. Process.*, 2016, **42**, 98–101.
- 32 S. S. Mali, H. Kim, W. Y. Jang, H. S. Park, P. S. Patil and C. K. Hong, *ACS Sustainable Chem. Eng.*, 2013, **1**, 1207–1213.
- 33 A. Tiwari, N. V. Krishna, L. Giribabu and U. Pal, *J. Phys. Chem. C*, 2018, **122**, 495–502.
- 34 L. Alagna, A. Capobianchi, M. P. Casaletto, G. Mattogno, A. M. Paoletti, G. Pennesi and G. Rossi, *J. Mater. Chem.*, 2001, **11**, 1928–1935.
- 35 F. Chindeka, P. Mashazi, J. Britton, D. O. Oluwole, S. Mapukata and T. Nyokong, *J. Photochem. Photobiol., A*, 2020, **399**, 112612.
- 36 B. D. Viezbicke, S. Patel, B. E. Davis and D. P. Birnie, *Phys. Status Solidi B*, 2015, **252**, 1700–1710.
- 37 Z. Huang, B. Zheng, S. Zhu, Y. Yao, Y. Ye, W. Lu and W. Chen, *Mater. Sci. Semicond. Process.*, 2014, **25**, 148–152.
- 38 C. Dette, M. A. Pérez-Osorio, C. S. Kley, P. Punke, C. E. Patrick, P. Jacobson, F. Giustino, S. J. Jung and K. Kern, *Nano Lett.*, 2014, **14**, 6533–6538.
- 39 S. Bagheri, K. Shamel and S. B. A. Hamid, *J. Chem.*, 2013, 1–5.
- 40 C. Z. Wen, H. B. Jiang, S. Z. Qiao, H. G. Yang and G. Q. Lub, *J. Mater. Chem.*, 2011, **21**, 7052–7061.
- 41 W. Muhammad, N. Ullah, M. Haroon and B. H. Abbasi, *RSC Adv.*, 2019, **9**, 29541–29548.
- 42 K. Hadjiivanov, *Adv. Catal.*, 2014, **57**, 99–318.
- 43 G. Soler-Illia, A. Louis and C. Sanchez, *Chem. Mater.*, 2002, **14**, 750–759.
- 44 A. K. Zak, R. Razali, W. H. A. Majid and M. Darroudi, *Int. J. Nanomed.*, 2011, **6**, 1399–1403.
- 45 H. Cheng, J. Wang, Y. Zhao and X. Han, *RSC Adv.*, 2014, **4**, 47031–47038.
- 46 S. Xu, S. Hartvickson and J. X. Zhao, *ACS Appl. Mater. Interfaces*, 2011, **3**, 1865–1872.
- 47 M. Managa, J. Britton, E. Prinsloo and T. Nyokong, *J. Coord. Chem.*, 2016, **69**, 3491–3506.
- 48 H. Ramesh, T. Mayr, M. Hobisch, S. Borisov, I. Klimant, U. Krühne and J. M. Woodley, *J. Chem. Technol. Biotechnol.*, 2016, **91**, 832–836.
- 49 T. Nyokong and E. Antunes, *In the handbook of porphyrin science*, ed. K. M. Kadish, K. M. Smith and R. Guillard, Academic Press, New York, 2010, pp. 247–349.
- 50 O. L. Osifeko, M. Durmuş and T. Nyokong, *J. Photochem. Photobiol., A*, 2015, **301**, 47–54.
- 51 S. E. Maree and T. Nyokong, Syntheses and photochemical properties of octasubstituted phthalocyaninato zinc complexes, *J. Porphyrins Phthalocyanines*, 2001, **5**, 782–792.
- 52 N. A. Youssef, S. A. Shaban, F. A. Ibrahim and A. S. Mahmoud, *Egypt. J. Pet.*, 2016, **25**, 317–321.
- 53 S. Al-Qaradawi and S. R. Salman, *J. Photochem. Photobiol., A*, 2002, **148**, 161–168.
- 54 C. L. Wang, L. Kong, X. Yang, L. Wang, S. Zheng, F. Chen, F. Maizhi and H. Zong, *Chemosphere*, 2000, **41**, 303–309.
- 55 S.-L. Chen, X.-J. Huang and Z.-K. Xu, *Cellulose*, 2011, **18**, 1295–1303.
- 56 M. N. Rashed and A. A. El-Amin, *Int. J. Phys. Sci.*, 2007, **2**, 073–081.

- 57 J. Kaur, S. Bansal and S. Singhal, *Phys. B*, 2013, **416**, 33–38.
- 58 Y. Li, X. Li, J. Li and J. Yin, *Water Res.*, 2006, **40**, 1119–1126.
- 59 J. Z. Kong, A. D. Li, X. Y. Li, H. F. Zhai, W. Q. Zhang, Y. P. Gong, H. Li and D. Wu, *J. Solid State Chem.*, 2010, **183**, 1359–1364.
- 60 M. U. D. Sheikh, G. A. Naikoo, M. Thomas, M. Banoa and F. Khan, *New J. Chem.*, 2016, **40**, 5483–5494.
- 61 P. Khoza and T. Nyokong, *J. Coord. Chem.*, 2015, **68**, 1117–1131.
- 62 M. Saeed, S. Adeel, M. Ilyas, M. A. Shahzad, M. Usman, E. Haq and M. Hamayun, *Desalin. Water Treat.*, 2016, **57**, 12804–12813.
- 63 J. Abhilasha and V. Dipti, *J. Chil. Chem. Soc.*, 2017, **62**, 3683–3690.
- 64 J. L. Wang and L. J. Xu, *Crit. Rev. Environ. Sci. Technol.*, 2012, **42**, 251–325.
- 65 M. A. Fox and M. T. Dulay, *Chem. Rev.*, 1993, **93**, 341–357.
- 66 V. Raditoiu, A. Raditoiu, M. F. Raduly, V. Amariutei, I. C. Gifu and M. Anastasescu, *Coatings*, 2017, **7**, 229.
- 67 H. Kim, W. Kim, Y. Mackeyev, G.-S. Lee, H.-J. Kim, T. Tachikawa, S. Hong, S. Lee, J. Kim, L. J. Wilson, T. Majima, P. J. J. Alvarez, W. Choi and J. Lee, *Environ. Sci. Technol.*, 2012, **46**(17), 9606–9613.